Flow structures around rectangular cylinder in the vicinity of a wall

J.F. Derakhshandeh[1a] and Md. Mahbub Alam[*2]

[1]*School of Mechanical Engineering of University of Adelaide, Australia*
[2]*Institute for Turbulence-Noise-Vibration Interaction and Control, Shenzhen Graduate School,
Harbin Institute of Technology, Shenzhen 518055, China*

Abstract. A numerical study is conducted on the flow characteristics of a rectangular cylinder (chord-to-width ratio C/W = 2 - 10) mounted close to a rigid wall at gap-to-width ratios G/W = 0.25 - 6.25. The effects of G/W and C/W on the Strouhal number, vortex structure, and time-mean drag and lift forces are examined. The results reveal that both G/W and C/W have strong influences on vortex structure, which significantly affects the forces on the cylinder. An increase in G/W leads to four different flow regimes, namely no vortex street flow ($G/W < 0.75$), single-row vortex street flow ($0.75 \leq G/W \leq 1.25$), inverted two-row vortex street flow ($1.25 < G/W \leq 2.5$), and two-row vortex street flow ($G/W > 2.5$). Both Strouhal number and time-mean drag are more sensitive to C/W than to G/W. For a given G/W, Strouhal number grows with C/W while time-mean drag decays with C/W, the growth and decay being large between $C/W = 2$ and 4. The time-mean drag is largest in the single-row vortex street regime, contributed by a large pressure on the front surface, regardless of C/W. A higher C/W, in general, leads to a higher time-mean lift. The maximum time-mean lift occurs for $C/W = 10$ at $G/W = 0.75$, while the minimum time-mean lift appears for $C/W = 2$ at the same G/W. The impact of C/W on the time-mean lift is more substantial in single-row vortex regime. The effect of G/W on the time-mean lift is larger at a larger C/W.

Keywords: boundary layers; rectangular cylinder; Strouhal number; vortex shedding frequency

1. Introduction

In this paper, a laminar flow past 2D rectangular cylinder located in the vicinity of a wall is investigated. For the chosen test cases, different chord-to-width (C/W) and gap ratios (G/W) are considered. This problem has been associated with many industrial applications such as wind engineering, civil engineering, and heat transfer in electronic equipment.

The flow around a circular cylinder has been extensively studied experimentally and numerically during the past decades (Bearman 1984, Parkinson 1989, Zdravkovich 1997, Norberg 2001, Norberg 2003, Williamson and Govardhan 2004, Alam and Kim 2009, Alam 2014, Derakhshandeh *et al.* 2014, Derakhshandeh *et al.* 2014, Derakhshandeh *et al*. 2015, Alam 2016, Derakhshandeh *et al.* 2016). Alternating vortex shedding occurs from the cylinder when the Reynolds number Re (= UD/v) is sufficiently high, $Re > 50$, where U is the freestream velocity, D is the diameter and v is the kinematic viscosity of the flowing fluid. The shedding frequency is normalized as Strouhal number $St = fD/U$, where f is the vortex shedding frequency.

A number of studies have been carried out on a rectangular cylinder subjected to a uniform flow. The flow structure over a rectangular cylinder is quite different from

that over a circular cylinder because of the difference in the flow separation mechanism, separation being oscillating for the circular cylinder and fixed for the rectangular cylinder (Mills *et al.* 2002, Alam *et al.* 2002, Zheng and Alam 2017).

The separation mechanism impacts on the shedding frequency as well as aerodynamic forces (Alam *et al.* 2011). The flow structure and dynamic behaviour of vortices from a rectangular cylinder can also be altered by changing the chord-to-width ratio C/W of the rectangular cylinder (Hourigan *et al.* 2001, Mills *et al*. 2003). The associated fluid dynamics become more complex for a cylinder mounted in a vicinity of a rigid wall, as the wall-to-cylinder gap ratio G/W gets involved in the flow.

A circular cylinder mounted in the vicinity of a rigid wall undergoes a number of different fluidic instabilities. Many of the previous investigations were conducted on the flow over a circular cylinder at relatively high Re, whereas the fluidic parameters of the flow are comparatively less sensitive to Re (Price *et al.* 2002, Re = 1200-4960; Sarkar and Sarkar 2010, Re =1440; Derakhshandeh *et al.* 2014a, Re = 8700). Similar studies have been conducted on the flow around square cylinders, again at high Re (Durao 1991, Re = 1.36×10^4, Bosch *et al.* 1996, Re = 2.2×10^4, Martinuzzi *et al.* 2003, Re = 1.89×10^4). Sohankar *et al.* (1999) using finite volume (FV) analysis identified two modes, known as modes A and B, in their numerical simulations. Martinuzzi *et al.* (2003) at Re = 1.89×10^4 measured time-mean and fluctuating surface pressure on a square cylinder with G/W varying from 0.07 to 1.6. The flow and the vortex shedding strength are similar to the no-wall case for $G/W > 0.9$. For $0.3 < G/W < 0.9$, the wall exerts a greater influence on the flow. The time-mean drag and the

---

*Corresponding author, Professor
 E-mail: alam@hit.edu.cn
[a] Research associate
 E-mail: javad.farrokhiderakhshandeh@adelaide.edu.au

Table 1 Selected studies on flow over circular and square cylinders highlighting the critical *G/W*

Scholars	Cylinder	*Re*	*G/W*	$(G/W)_{crt}$
Grass *et al.* (1984)	Circular	$2.24\text{-}4.32\times10^3$	0.28, 6	0.25-0.3
Taniguchi and Miyakoshi (1990)	Circular	9.4×10^4	0.34-1.05	0.3-0.9
Buresti and Lanciotti (1992)	Circular	$8.6\text{-}27.7\times10^4$	0.1-1.1	0.3
Lei *et al.* (1999)	Circular	$13\text{-}14.5\times10^3$	0.14-2.89	0.5
Sarkar and Sarkar (2010)	Circular	1.44×10^3	0.25-1.0	0.5
Wang *et al.* (2013)	Circular	$3\text{-}13\times10^3$	0.05-2.5	0.3
Durao *et al.* (1988)	Square	13.6×10^3	0.8	0.35
Bosch *et al.* (1996)	Square	22×10^3	0.13	0.35-0.5
Wu (1999)	Square	23×10^3	1.5	0.3-0.5
Martinuzzi *et al.* (2003)	Square	18.9×10^3	0.5	0.3-0.5
Mahir (2009)	Square	< 250	0.2-4	0.5

strength of the shed vortices decrease as *G/W* is reduced from 0.9 to 0.6. The circulation of vortices in the wake of the square cylinder appears to be directly related to the periodic loading of the cylinder. On the other hand, for *G/W*< 0.3D, the periodic activity of the flow is fully suppressed in the near wake region.

Mills *et al*. (2003) performed a series of particle image velocimetry measurements in a closed loop water channel for the flow around a rectangular cylinder at *Re* = 490. The results revealed that the growth of vortices at the trailing edge is weaker as compared with the leading edge vortices. This is due to the interaction of the trailing and leading edge vortices generated at a similar phase in the perturbation cycle. Nakamura *et al.* (1991) experimentally investigated vortex shedding from rectangular cylinders of *C/W* = 2 - 16. It was found that the Strouhal number is approximately constant at 0.6 for *C/W* = 3-5. They also showed that a further increase in *C/W* causes an increment in *St*, which is equal to integer multiples of 0.6. Later, the relationship between the *C/W* and *St* has been numerically confirmed by Tan *et al.* (2003).

A number of studies have been conducted on flow over circular and square cylinders at high *Re*. Some selected are presented in Table 1, highlighting the critical *G/W* below which the alternating vortex shedding is suppressed. It is seen that for the most of the studies, the critical gap ratio ranges between 0.3 and 0.5. However, studies on a square or rectangular cylinder at low *Re* are very limited.

Two and three-dimensional numerical studies were conducted by Mahir (2009) at *Re* = 175-250 for the flow over a square cylinder near a wall. The effect of *G/W* was considered. It was found that at *G/W* = 0.5 the Strouhal numbers for both two and three-dimensional models are similar. The maximum lift and drag coefficients were achieved for *G/W* < 1. Mahir (2009) did not consider the effect of *C/W* on the flow of forces.

The objective of this study is to investigate the flow past a rectangular cylinder in the vicinity of the rigid wall in order to find the relationship between the Strouhal number, *C/W* (= 2-10) and *G/W* (= 0.25-6.25). The vortex structure and forces on the rectangular cylinder at different *G/W* and *C/W* are analyzed and presented. A series of numerical simulations of two-dimensional flow over rectangular cylinders is performed for *C/W* and *G/W* ranges considered.

2. Governing equations and numerical method

The numerical simulations were modeled in ANSYS Fluent using the Lagrangian solution of two-dimensional Navier-Stokes equations. The solution was based on the second order implicit Finite Volume Method (FVM) to achieve a better approximation as compared with the first order. The governing equations including continuity and momentum for an unsteady viscous laminar fluid flow can be written as

$$\frac{\partial u}{\partial x} + \frac{\partial v}{\partial x} = 0 \tag{1}$$

$$\left.\begin{array}{l} \dfrac{\partial u}{\partial t} + u\dfrac{\partial u}{\partial x} + v\dfrac{\partial u}{\partial y} = -\dfrac{1}{\rho}\dfrac{\partial P}{\partial x} + \nu(\dfrac{\partial^2 u}{\partial x^2} + \dfrac{\partial^2 u}{\partial y^2}), \ \text{ and} \\[2ex] \dfrac{\partial v}{\partial t} + u\dfrac{\partial v}{\partial x} + v\dfrac{\partial v}{\partial y} = -\dfrac{1}{\rho}\dfrac{\partial P}{\partial x} + \nu(\dfrac{\partial^2 v}{\partial x^2} + \dfrac{\partial^2 v}{\partial y^2}) \end{array}\right\} \tag{2}$$

where *u* and *v* are the velocity components in the *x* and *y* directions, respectively, *P* is the static pressure, *t* is the time, and ν is the kinematic viscosity of the fluid.

The Computational domain and boundary conditions considered in this study are presented in Fig. 1. The boundary conditions applied at the computational domain were defined as: uniform velocity at the inlet boundary, no-slip on the surface of the cylinder and the rigid wall, free-slip on the upper boundary, and zero velocity derivative at the outlet boundary. The thickness of the cylinder *W* was 8 mm while the gap *G* between the cylinder and rigid wall was varied as 2 mm, 6 mm, 10 mm, 20 mm and 50 mm, corresponding to *G/W* = 0.25, 0.75, 1.25, 2.5, 6.25, respectively.

The front surface of the cylinder was set 10*W* away from the inlet boundary (Fig. 1). The boundary layer thickness δ, defined as the distance from the wall to the location of *u* = 0.99*U*, at *x* = 10*W* was found to be 29.5 mm in the absence of the cylinder. Using Blasius equation, it is obtained as $\delta \approx 5x/Re_x^{1/2}$ = 28 mm, very close that obtained from the simulation.
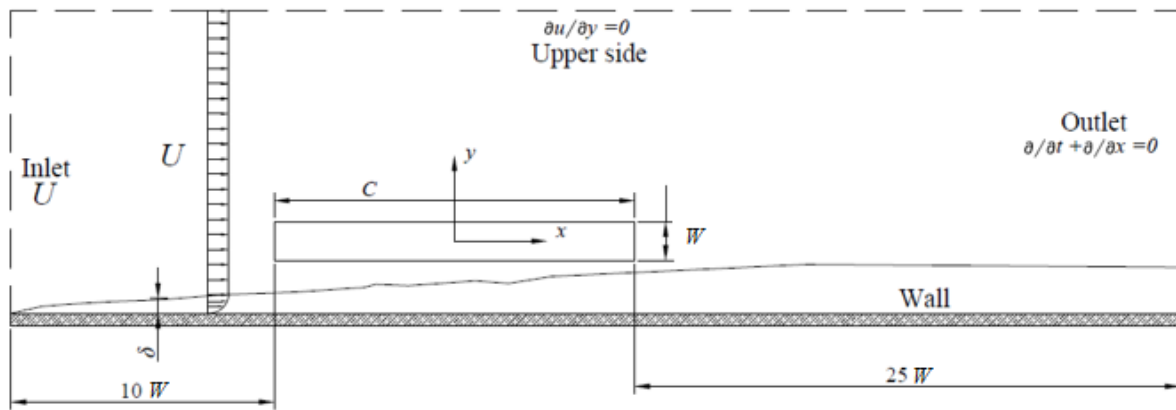
Fig. 1 Computational domain and boundary conditions for laminar flow around a rectangular cylinder in the vicinity of a wall

As a result, the cylinder is fully or partially submerged in the boundary layers when G varies from 2 to 20 mm. At $G = 50$ mm, the cylinder is completely outside of the boundary layers. With keeping W constant, the chord C of the cylinder is varied as $C/W = 2, 4, 6, 8$ and 10. Therefore, a total of 25 simulations are carried out as listed in Table 2. For all test cases, the Re based on W and freestream velocity U (=0.365 m/s) at the inlet was 200, chosen to guarantee the vortex street as well as to avoid three-dimensionality in the flow (Tan *et al.* 2003, Sohankar and Etminan 2009).

Table 2 Test cases showing values of *C/W* and *G/W*

Groups	Test Case	C/W	G/W
1	1	2	0.25
	2	2	0.75
	3	2	1.25
	4	2	2.5
	5*	2	6.25
2	6	4	0.25
	7	4	0.75
	8	4	1.25
	9	4	2.5
	10*	4	6.25
3	11	6	0.25
	12	6	0.75
	13	6	1.25
	14	6	2.5
	15*	6	6.25
4	16	8	0.25
	17	8	0.75
	18	8	1.25
	19	8	2.5
	20*	8	6.25
5	21	10	0.25
	22	10	0.75
	23	10	1.25
	24	10	2.5
	25*	10	6.25

*Cylinder lying outside the boundary layer

3. Mesh structure and grid resolution tests

In the numerical models, we employed structured meshes. Four mesh resolutions were examined for one typical test case $C/W = 10$, the largest cylinder. The method of Grid Convergence Index (GCI) recommended by Celik *et al.* (2008) was exploited to identify that the selected resolution is sufficient to precisely capture the flow characteristics, particularly in boundary layers close to the rigid wall and around the cylinder. Fig. 2 depicts typically structured meshes for the largest C/W with the minimum gap ratio ($G/W = 0.25$). The time step was determined to be 0.002 s that satisfies the convergence criteria and Courant constraint. Based on U and W, the non-dimensional time step is 0.091. The simulations were conducted for about 10 s while converging before ≈ 2.5 s. A sampling time of 2.5 – 10 s was used to calculate the statistics such as time-mean drag, time-mean lift, and power spectrum.

Table 3 summarizes St, time-mean drag ($\overline{C}_D$) and rms lift coefficient ($C_{L, rms}$) as a function of grid number (N_g). The results reveal that St, $\overline{C}_D$ and $C_{L, rms}$ converge for mesh case 3 (MC$_3$), with a percentage of error of 1%, 1.6%, and 1.5%, respectively. Hence, for the rest of the simulations, MC$_3$ is chosen.

4. Results and discussion

4.1 Reproduction of Strouhal number for unbounded cylinder

In order to further verify the numerical results, the flow around the unbounded cylinder of different C/W was considered at $Re = 200$, and the variation of Strouhal number is compared in Fig. 3. Here St_c represents the Strouhal number, which is evaluated based on C. Typical power spectra of the lift forces as a function of C/W are illustrated in Fig. 3(a).
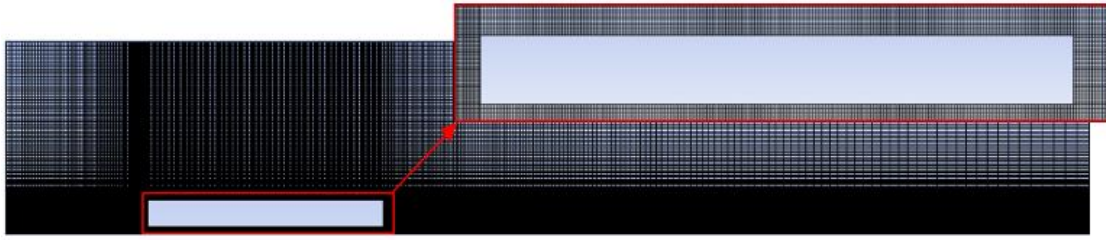
Fig. 2 A typical two-dimensional structured mesh around the rectangular cylinder with *C/W* = 10 and *G/W* = 0.25

Table 3 Typical mesh refinement test for *C/T* = 10 and *G/W* = 0.25

Mesh Case	Mesh quality	N_g	St	% error	$C_{L,rms}$	% error	$\overline{C}_D$	% error
MC_1	Very Coarse	38,688	1.810	6.2%	0.101	15.8%	0.175	9.7%
MC_2	Coarse	49,746	1.870	3.1%	0.108	10.0%	0.186	4.1%
MC_3	Refined	57,211	1.910	1.0%	0.118	1.6%	0.191	1.5%
MC_4	Highly refined	61,442	1.930	---	0.120	---	0.194	---
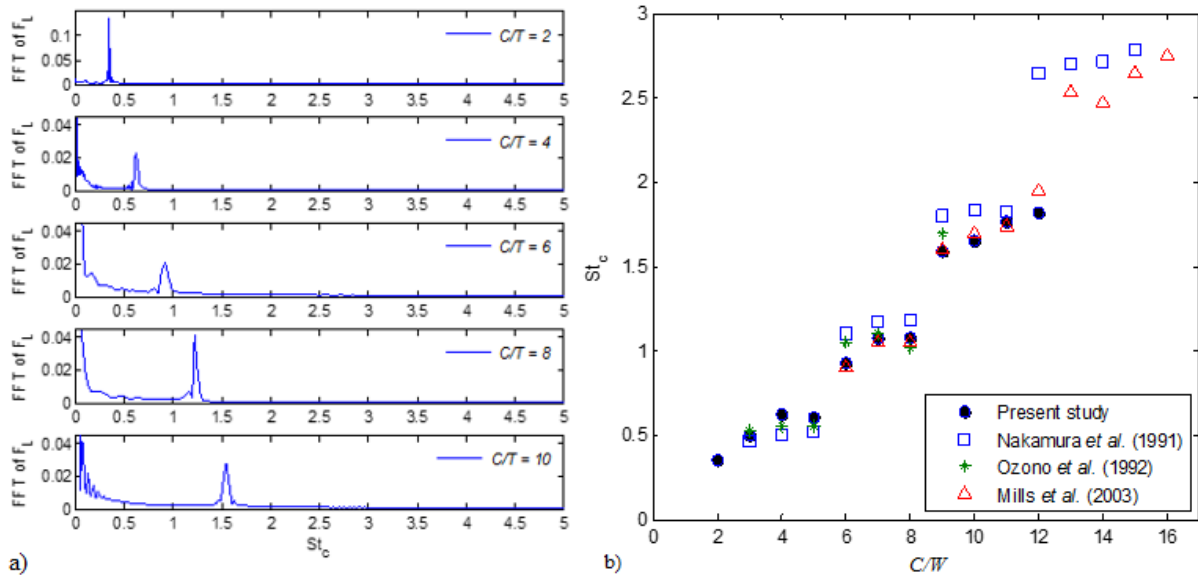
Fig. 3 (a) Power spectra of lift force for typical *C/W*, and (b) dependence of St_c on *C/W*

The power spectra reveal that an increase in *C/W* leads to a jump in St_c step-by-step. With $St_c = 0.35$ at *C/W* = 2, St_c jumps between *C/W* = 2 and 3, lying constant at ≈ 0.55 over *C/W* = 4-5. The St_c leaps to higher values with a further increase in *C/W*, which are almost equal to integral multiples of 0.55. Numerical investigations conducted by Tan *et al.* (2003) for the flow around a rectangular cylinder revealed that St_c can be formulated as $St_c = 0.55n$. Here, the "*n*" is an integer number and stands for the number of vortices along the rectangular cylinder. The results demonstrate that the St_c(s) for all test cases are in good agreement with the previous numerical studies.

4.2 Vortex shedding in the wake of the cylinder

Figs. 4 and 5 show dependence of *G/W* on typical vorticity structures at *C/W* = 6 and 10, respectively. The normalized vorticity $\omega_z^* (=\omega_z W/U)$ contours represent a comprehensive physical behavior of the flow and vortex pattern, where ω_z is the vorticity in the *z*-direction. Red and green colors in the figures represent the maximum (positive) and the minimum (negative) vorticity, respectively. The vortices cause a pressure fluctuation and a flow velocity alteration around and in the near wake of the cylinder (Derakhshandeh *et al.* 2014b). At *G/D* = 0.25 (Fig. 4(a)), there is no vortex shedding from the cylinder, the shear layers persisting to be stable. A similar observation was
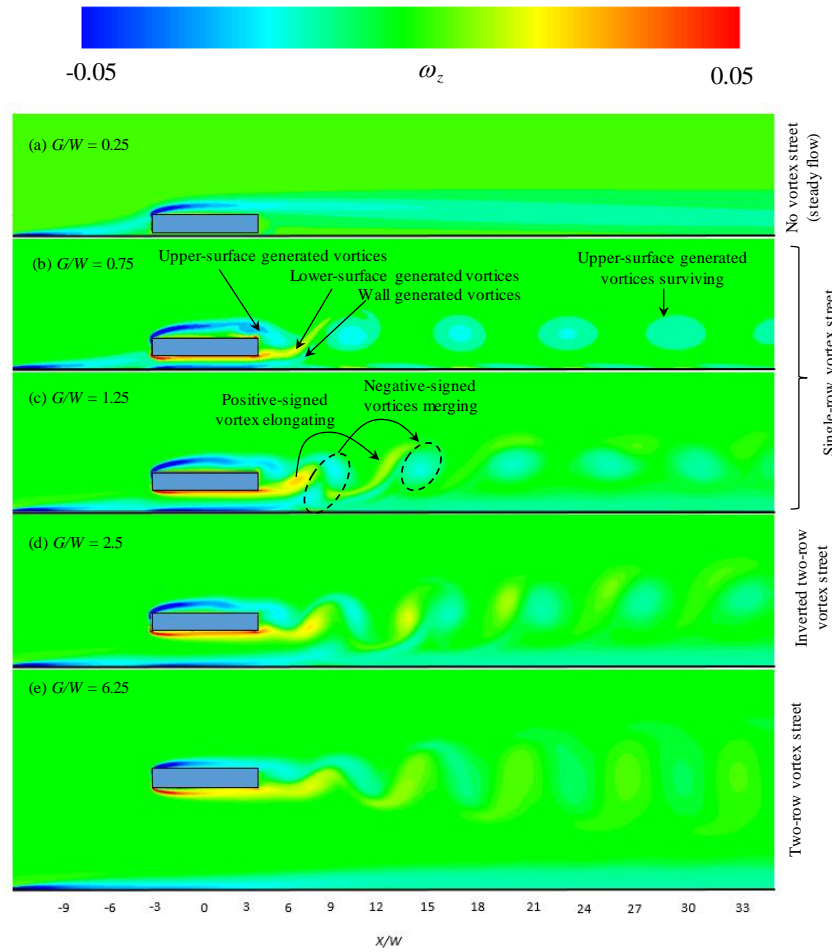
Fig. 4 Dependence of vorticity structure on *G/W*. Red and green colors represent the maximum (positive) and the minimum (negative) vorticity, respectively. *C/W* = 6

made for the other *C/W* (e.g., Fig. 5(a)). This means that *G/W* plays a more important role than *C/W*.

At *G/W* = 0.75 - 1.25, vortex shedding occurs from both freestream side and gap; the feature is different from that for *G/W* = 0.25 (Figs. 4(b) and 4(c)). In the gap, two boundary layers are developed, one by the wall and the other by the lower surface of the cylinder, generating two counter-rotating vortices behind the cylinder. The positive-signed vortex originating from the lower surface of the cylinder is elongated outwards as a jet flow. On the other hand, the upper shear layer reattaches near the trailing edge of the cylinder, shedding negative-signed vortices. Having a higher velocity because of the jet-like flow from the gap, the two vortices from the gap approach the vortex from the upper shear layer and interact. Because of having the same-sign of vorticity, the vortices from the upper side and wall merge together (Fig. 4(c)). The ensuing vortex thus gets bigger in size. As the positive-signed vortex shed from the lower surface lies between the vortices from the wall and lower surface, it elongates and moves to the freestream side due to the clockwise rotation of the combined vortex. The elongated vortex decays rapidly and loses its identity downstream. A single-row vortex street thus characterizes the wake.

At *G/W* = 2.5, the thickness of the boundary layer is approximately $\delta/W \approx 1$. This means the bottom surface of the cylinder just touches the wall boundary layer. As the two boundary layers in the gap are separated enough, the interaction between vortices from the upper surface and wall is feeble. The vortices from the lower surface thus can survive in the wake, albeit moving toward the freestream side. Eventually, the anticlockwise and clockwise vortices take place on the upper and lower sides of the wake, respectively, the vortex orientation being opposite to that in the classical Karman vortex street. The street forming in the wake here is termed as inverted two-row vortex street.

At *G/W* = 6.25, there is no interaction between the vortices from the cylinder and from the wall, the influence of the wall on the cylinder wake is negligible. The vortices shedding from the cylinder appear in a symmetric pattern, forming a two-row Karman vortex street. A similar observation is made for *C/W* = 10 (Fig. 5), albeit the influence of *C/W* cannot be neglected. For example, at *G/W* = 0.75 and 1.25, while vortices from the wall boundary layer and cylinder lower-side boundary layer for *C/W* = 6 are comparable to each other (Fig. 4), vortex from the wall for *C/W* = 10 is weaker than that from the cylinder.
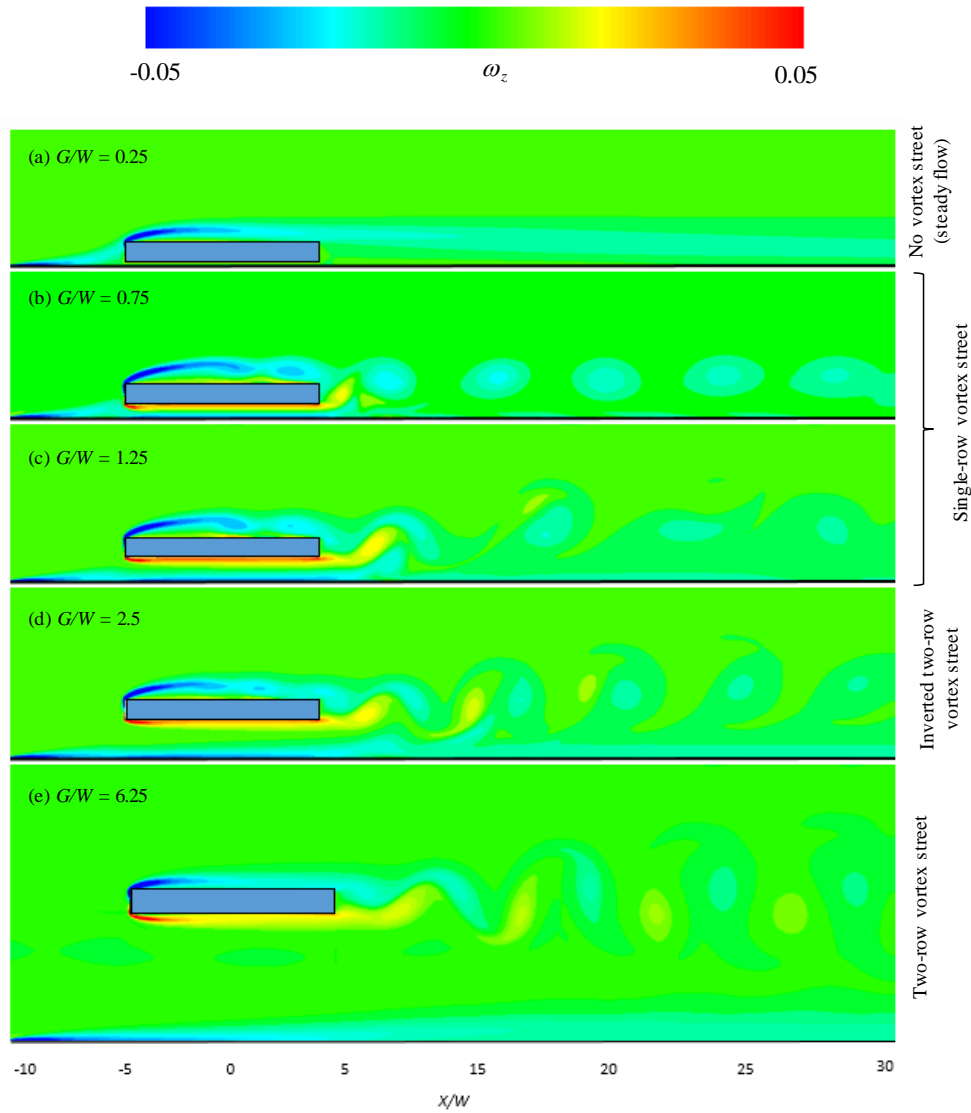
Fig. 5 Dependence of vorticity structure on *G/W*. Red and green colors represent the maximum (positive) and minimum (negative) vorticities, respectively. *C/W* = 10

Fig. 6 shows the time series of lift coefficient C_L of the cylinder (left column) for *C/W* = 6, exploring further evidence of the claim made above. While constant for *G/W* = 0.25, C_L after the convergence oscillates for *G/W* = 0.75 due to alternating vortex shedding from the two sides of the cylinder. No peak in the power spectra (right column) is discernible for *G/W* = 0.25, but a clear peak emerges for *G/W* = 0.75. Further increasing the gap ratio up to *G/W* = 6.25 not only causes a reduction in the amplitude of the fluctuating C_L but also leads to a reduction in the mean C_L. The amplitude of C_L is maximum at *G/W* = 0.75 where the gap vortices vigorously interact with the freestream side vortices. With increasing *G/W* from 0.75, as the interaction gets feeble, the amplitude of C_L follows suit.

To gain more insight into the frequency response of the vortices, variations in St_c as a function of *C/W* is also plotted in Fig. 7. An unbounded cylinder St_c is also included for a comparison purpose. For all the cases, St_c grows with *C/W*. The St_c for *G/W* = 6.25 follows the unbounded cylinder results, implying that the cylinder with *G/W* behaves an unbounded cylinder regardless of *C/W*. Interestingly, compared to the counterpart in the unbounded cylinder, St_c is smaller for *G/W* = 0.75 but larger for *G/W* = 1.25 and 2.5. The smaller St_c at *G/W* = *0.75* is attributed to the fact that the cylinder lies in the boundary layer developed by the wall. On the other hand, at *G/W* = 1.25 and 2.5, the shear layer velocity in the gap may be higher because of the flow blockage by the wall, leading to the larger St_c. For a circular or square cylinder placed in wind or water tunnel, it has been found that the Strouhal number increases when blockage ratio increases from 6% (Lee 1975, West and Appelt 1982, Zdravkovich 1997). The St_c for 3 ≤ *C/W* ≤ 8 at *G/W* = 1.25 and 2.5 is approximately 20-30% (depending on *C/W*) higher than that of the unbounded cylinder.
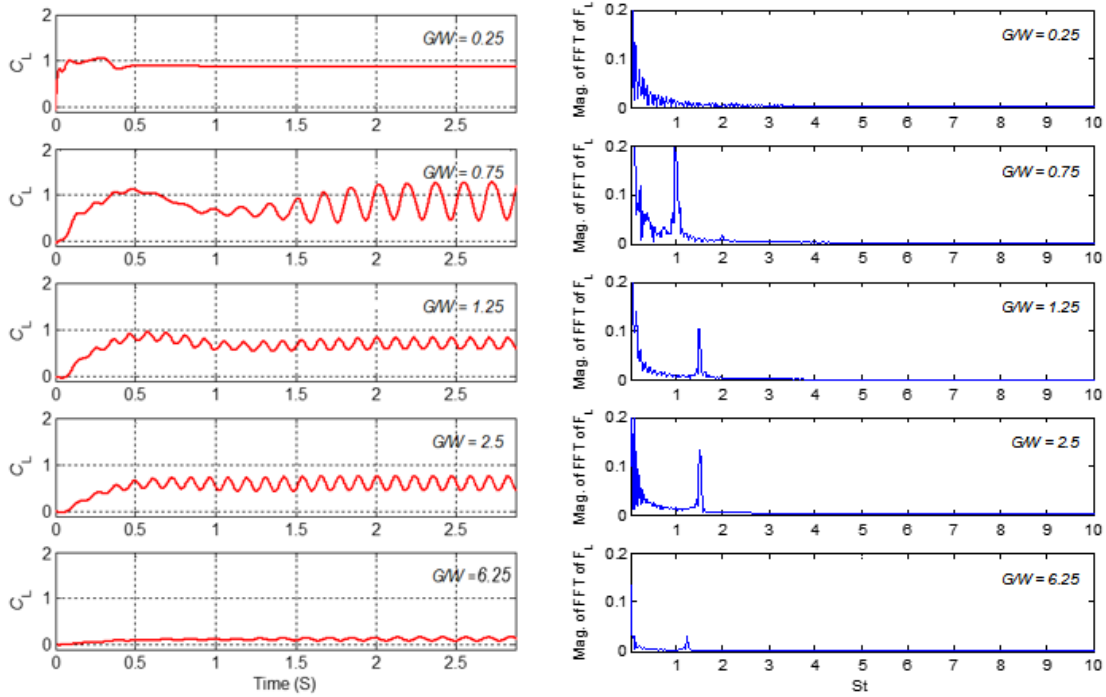
Fig. 6 Time histories of lift coefficient (left column) and power spectrum of fluctuating lift (right column). *C/W* = 6
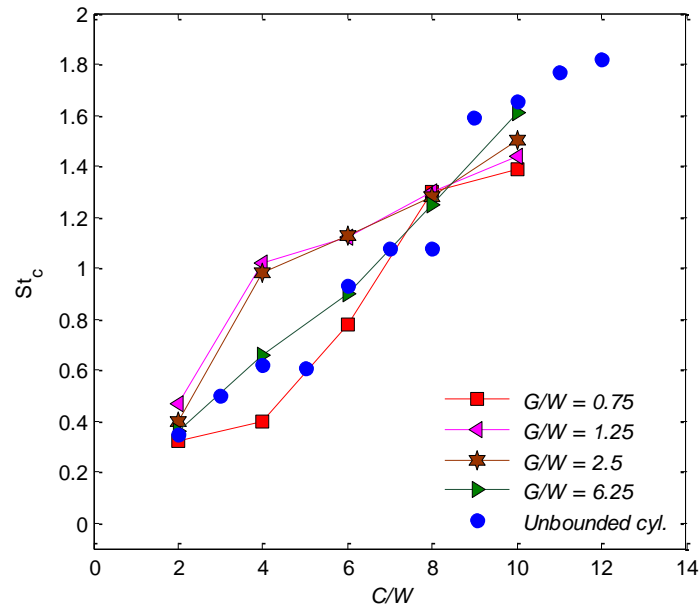

Fig. 7 Variation in the Strouhal number as a function of *C/W* and *G/W*

The dependence of St_c on *G/W* can be observed in Fig. 8 and can be linked to the four flow regimes identified above. Under the influence of *G/W*, the St_c behaves differently and its variation cannot be formulated explicitly as an unbounded cylinder (Fig. 3). An increase in St_c is identified between *G/W* = 0.75 and 1.25 for *C/W* = 2-6. At these small *G/W*, the change in St_c for higher *C/W* = 8 and 10 is insignificant, suggesting that at a higher *C/W* the vortex shedding from the cylinder is less influenced by the wall

boundary layer. The observation is consistent with the observation made in Figs. 4 and 5 that at *G/W* = 0.75 and 1.25 vortex from the wall is weaker than that from the cylinder for *C/W* = 10 but comparable to *C/W* = 6. For *G/W* ≥ 2.5, St_c is almost insensitive to *G/W*. The St_c is more sensitive to *C/W* than to *G/W*, increasing with *C/W* for a given *G/W*. The increase is, however, largest between *C/W*= 2 and 4.
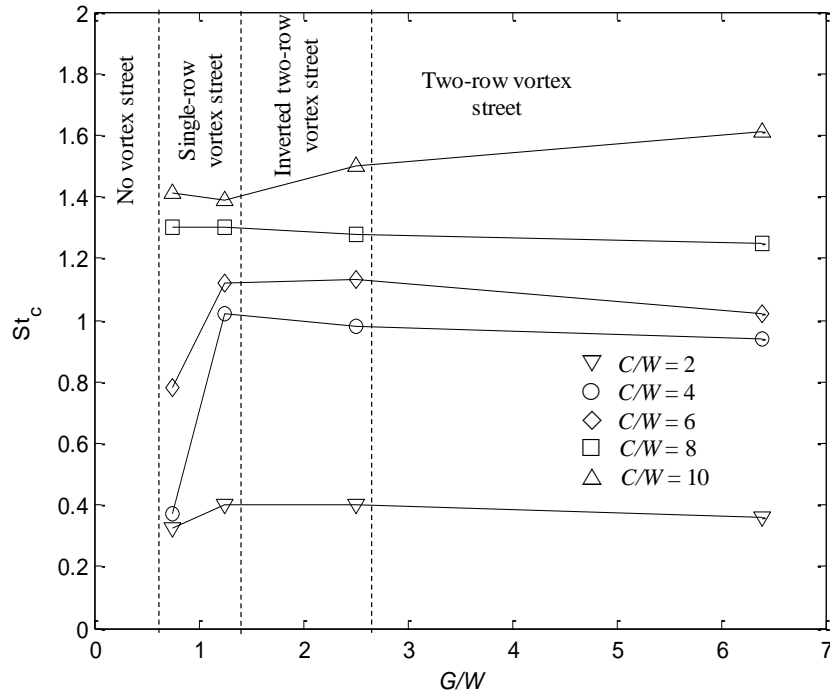
Fig. 8 Effect of *G/W* on Strouhal number at different *C/W*
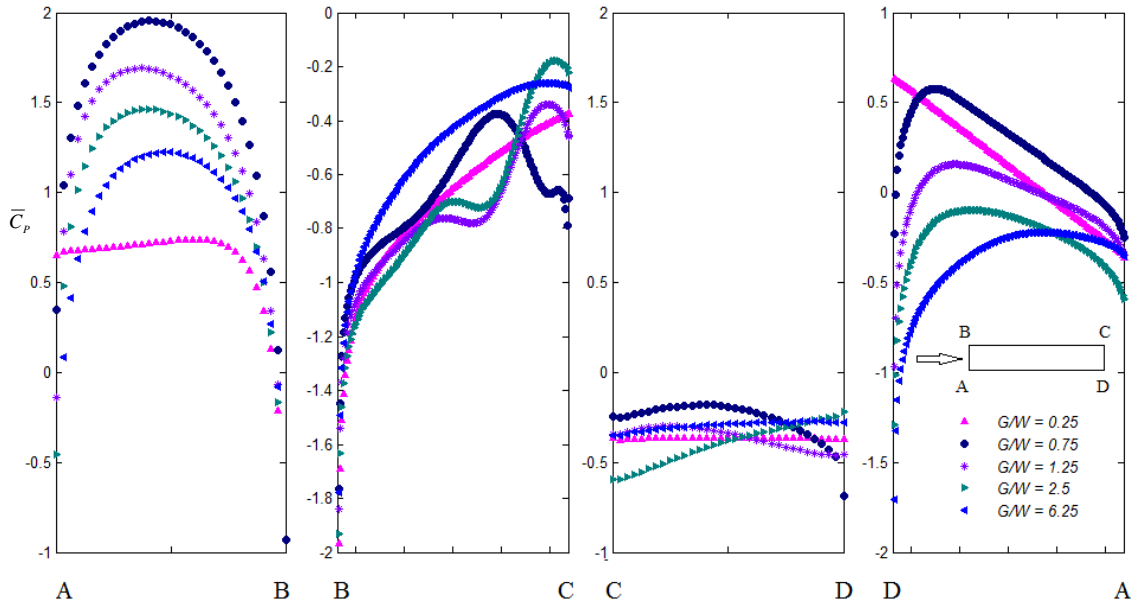
Fig. 9 Time-mean pressure coefficient $\overline{C}_P$ on the surfaces of the cylinder, *C/W* = 6

4.3 Pressure distribution around the cylinder

Fig. 9 shows the time-mean pressure coefficient $\overline{C}_P$ distributions on the four surfaces of the cylinder. The $\overline{C}_P$ on the front surface (A-B) for *G/W* = 0.25 is smaller than 1.0 because of the cylinder lying in the wall boundary layer thickness and no vortex shedding occurring from the cylinder. At *G/W* = 0.75, the outer edge of the wall boundary layer incidents slightly below (maximum $\overline{C}_P$ position) the nominal stagnation point on the front surface, leading to a very large $\overline{C}_P$ on the front surface. With increasing *G/W* from 0.75 to 1.25, the maximum $\overline{C}_P$ on the front surface decreases and the position of the maximum $\overline{C}_P$ shifts towards the lower edge A. As the cylinder is away from the wall boundary layer with *G/W* increasing

from 2.5, the maximum $\overline{C}_P$ position moves toward the nominal stagnation point. At the largest $G/W = 6.25$ examined, the $\overline{C}_P$ distribution becomes symmetric with a maximum $\overline{C}_P$ occurring at the nominal front stagnation point, very similar to that on the unbounded cylinder (not shown). Along the upper surface (B-C), $\overline{C}_P$ escalates being very low at the corner B, which indicates that the flow separation occurs at the leading edge. The peak appearing near the trailing edge for $G/W \geq 0.75$ suggests the reattachment of the upper shear layer (Fig. 4). On the rear surface (C-D), $\overline{C}_P$ distribution is flat for $G/W = 0.25$ because of steady flow. Interestingly, $\overline{C}_P$ for $G/W = 0.75$ and 1.25 (single-row vortex street) is smaller around the lower corner D than around the upper corner C, confirming that the gap flow for these G/W acts as a jet. The associated vortices can thus come close to the vortices from the upper shear layer, interact vigorously and vanish, which explains why single-row vortex street forms in the wake. On the other hand, the $\overline{C}_P$ variation along the surface for $G/W = 2.5$ and 6.5 (two-row vortex street) is opposite to that for $G/W = 0.75$ and 1.25, $\overline{C}_P$ being smaller at corner C.

On the bottom surface (A-D), the highly negative $\overline{C}_P$ at the corner D for $G/W = 0.75$-6.25 insinuates the occurrence of the flow separation. The flow from the lower corner is not separated for $G/W = 0.25$. The $\overline{C}_P$ distributions for $G/W = 0.75$-6.25 display a peak each, the peak shifting toward the trailing edge with increasing G/W. This peak is generated due to the reattachment of the shear layer (Fig. 4).

In summary, G/W has more impact on $\overline{C}_P$ on the front and lower surfaces than on the rear and upper surfaces, respectively.

4.4 Lift and drag forces

The effect of G/W on the pressure distribution around the cylinder was studied in the previous section. The surface pressure can be suitably highlighted by the drag and lift forces. Consequently, in this section, the drag and lift coefficients are studied and evaluated.

The dependence on G/W of the time-mean drag coefficient $\overline{C}_D$ for different C/W is illustrated in Fig. 10(a). Again the flow regimes are marked in the figure. In the no vortex street regime, $\overline{C}_D$ for a given C/W is small and sharply increases with G/W. $\overline{C}_D$ becomes maximum in the single-row vortex street regime where the interaction between the upper side and gap vortices is the strongest. Due to the weakening interaction, $\overline{C}_D$ declines with G/D in inverted two-row vortex street and generated two-row vortex street regimes. Interestingly, given the same G/W, an increase in C/W corresponds to a decrease in $\overline{C}_D$. The decrease is, however, very large between $C/W = 2$ and 4.

The effect of G/W on the time-mean lift coefficient $\overline{C}_L$ is presented in Fig. 12(b). In general, a higher C/W corresponds to a higher $\overline{C}_L$ in the no vortex, single-row vortex and inverted two-row vortex street regimes. Maximum $\overline{C}_L$, however, prevails at $C/W = 10$, $G/W = 0.75$. At this G/W, this maximum value tappers off with decreasing C/D, getting minimum for $C/W = 2.0$. At the higher G/W examined, $\overline{C}_L$ is almost independent of C/W. Interestingly, the influence of C/W is more substantial in the single-row vortex regime, for instance, at $G/W = 0.75$, $[\overline{C}_L]_{C/W=10} \approx 10.5 \times [\overline{C}_L]_{C/W=2}$. On the other hand, the effect of G/W is the greatest for $C/W = 10$.

5. Conclusions

A 2D laminar flow past a rectangular cylinder mounted in a vicinity of a rigid wall is simulated to study the physical feature of the flow at $Re = 200$ based on W. Chord-to-width ratios (C/W) for the rectangular cylinder is varied from 2 to 10 and the gap spacing ratio (G/W) between the cylinder and wall is changed from 0.25 to 6.25. The results reveal that both G/W and C/W have strong influences on vortex structure. As such four different flows are identified based on the dynamic behaviour of the vortices, i.e., no vortex street flow, single-row vortex street flow, inverted two-row vortex street flow, and two-row vortex street flow. The no vortex street flow occurring at $G/W < 0.75$ is steady, no vortices generated in the wake. The single-row vortex flow ($0.75 \leq G/W \leq 1.25$) features a single row of negative vortices. Two opposite-signed vortices (one by the wall and the other by the lower surface of the cylinder) from the gap come into being against one vortex shed from the upper surface in one period. The vortex from the wall merges with that the upper surface, forming a combined vortex. The vortex from the lower surface of the cylinder exhausts because of a strong interaction with the vortices from the wall and upper surface. The combined vortices thus surviving in the wake generate a single-row street. In inverted two-row vortex street flow ($1.25 < G/W \leq 2.5$), the interaction between the lower surface vortex and the upper surface vortex and/or wall vortex is feeble. The vortices from the lower surface thus can survive, moving toward the freestream side. The upper and lower surface vortices take position oppositely in the wake, forming an inverted two-row vortex street. The two-row vortex street flow appearing at $G/W > 2.5$ is characterized by two single vortices shedding in one cycle, where the upper and lower surface vortices take positions in the upper and lower sides of the wake, respectively. The interaction between the vortices from the cylinder and from the wall is negligible.

The presence of the wall significantly influences the Strouhal number in the single-row and inverted two-row vortex streets. The Strouhal number is highly dependent on C/W, increasing with C/W. The increase is largest between $C/W = 2$ and 4. The Strouhal number for $G/W = 6.25$ follows that of the unbounded cylinder, regardless of C/W.
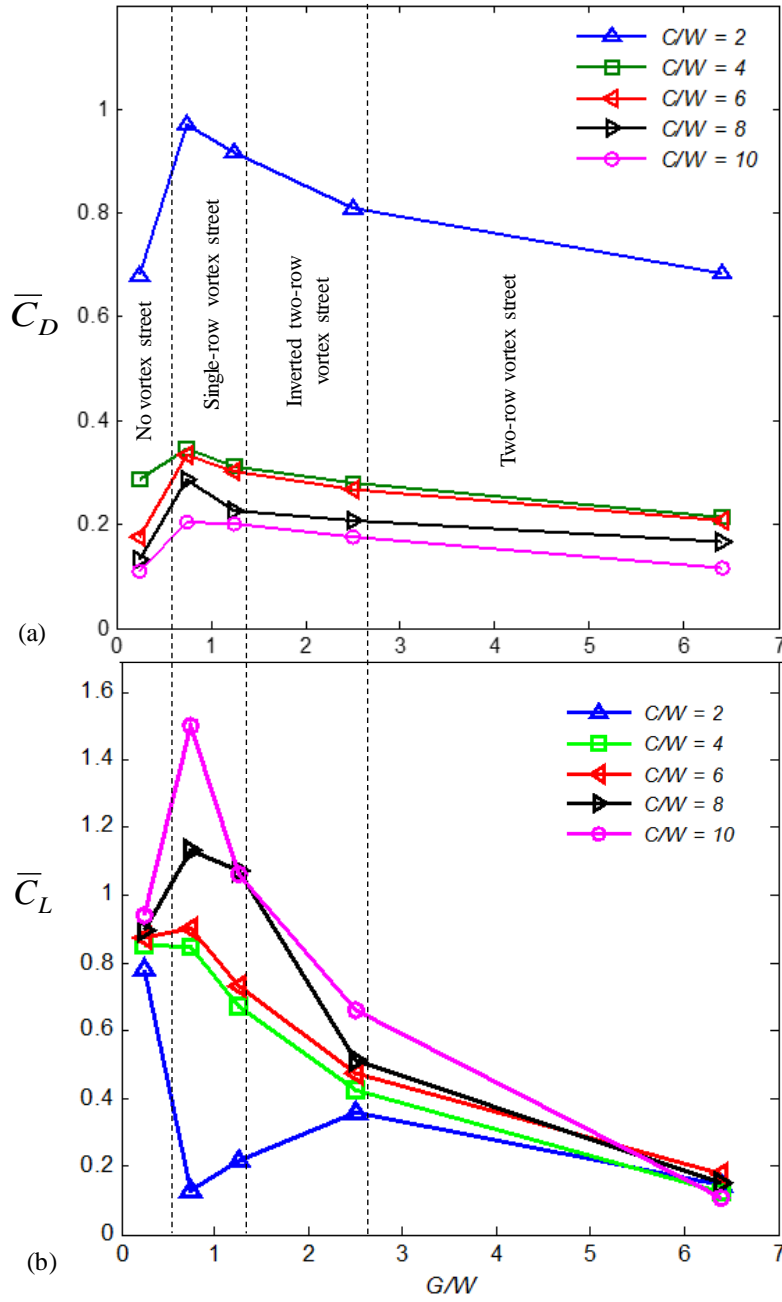
Fig. 10 Variations in (a) mean drag coefficient $\overline{C}_D$ and (b) time-mean lift coefficient $\overline{C}_L$ as a function of *G/W* and *C/W*

Compared to the counterpart in the unbounded cylinder, Strouhal number is smaller for *G/W* = 0.75 but larger for *G/W* = 1.25 and 2.5. The Strouhal number for $3 \leq C/W \leq 8$ at *G/W* = 1.25 and 2.5 is approximately 20-30% (depending on *C/W*) higher than that of the unbounded cylinder. The Strouhal number is more sensitive to *C/W* than to *G/W*, increasing with *C/W* for a given *G/W*.

Time-mean pressure on the front surface is the largest at *G/W* = 0.75 in the single-row vortex street flow as the outer edge of the wall boundary layer incidents on the front surface. With increasing *G/W* from 0.75 to 1.25, the maximum $\overline{C}_P$ on the front surface decreases and the

position of the maximum $\overline{C}_P$ shifts towards the lower edge. The pressure on the front and lower surfaces is more sensitive to *G/W* than that on the rear and upper surfaces, respectively. Regardless of *C/W*, $\overline{C}_D$ is largest in the single-row vortex street regime, contributed by a large pressure on the front surface. $\overline{C}_D$ decays with *G/W* in inverted two-row vortex street and two-row vortex street regimes. Given the same *G/W*, an increased *C/W* leads to a decreased $\overline{C}_D$, the decrease being very large between *C/W* = 2 and 4. A higher *C/W* corresponds to a higher $\overline{C}_L$ for a

given *G/W*. Maximum $\overline{C_L}$ occurs for *C/W* = 10 at *G/W* = 0.75, while minimum $\overline{C_L}$ appears for *C/W* = 2 at the same *G/W*. The impact of *C/W* is more substantial in the single-row vortex regime. The effect of *G/W* on $\overline{C_L}$ is larger at a larger *C/W*.

Acknowledgments

References

Alam, M.M. (2014), "The aerodynamics of a cylinder submerged in the wake of another", *J. Fluid. Struct.*, **51**, 393-400.

Alam, M.M. (2016), "Lift forces induced by phase lag between the vortex sheddings from two tandem bluff bodies", *J. Fluid. Struct.*, **65**, 217-237.

Alam, M.M. and Kim, S. (2009), "Free vibration of two identical circular cylinders in staggered arrangement", *Fluid Dynam. Res.*, **41**(3), 035507.

Alam, M.M., Moriya, M., Takai, K. and Sakamoto, H. (2002), "Suppression of fluid forces acting on two square prisms in tandem arrangement by passive control of flow", *J. Fluid. Struct.*, **16**, 1073-1092.

Alam, M.M., Zhou, Y. and Wang, X.W. (2011), "The wake of two side-by-side square cylinders", *J. Fluid. Mech.*, **669**, 432-471.

Bearman, P.W. (1984), "Vortex shedding from oscillating bluff bodies", *Annu. Rev. Fluid Mech.*, **16**(1), 195-222.

Bosch, G., Kappler, M. and Rodi, W. (1996), "Experiments on the flow past a square cylinder placed near a wall", *Exp. Therm. Fluid Sci.*, **13**(3), 292-305.

Buresti, G. and Lanciotti A. (1992), "Mean and fluctuating forces on a circular cylinder in cross-flow near a plane surface", *J. Wind Eng. Ind. Aerod.*, **41**(1-3), 639-650.

Celik, I.B., Ghia, U. and Roache, P.J. (2008), "Procedure for estimation and reporting of uncertainty due to discretization in CFD applications", *J. Fluids Eng. –T ASME*, **130**(7).

Derakhshandeh, J., Arjomandi M., Cazzolato B. and Dally B. (2014a), "Effect of a rigid wall on the vortex induced vibration of two staggered circular cylinders", *Renew. Sust. Energ.*, **6**(3), 033114.

Derakhshandeh, J., Arjomandi M., Dally B. and Cazzolato B. (2014b), "The effect of arrangement of two circular cylinders on the maximum efficiency of Vortex-Induced Vibration power using a Scale-Adaptive Simulation model", *J. Fluid. Struct.*, **49**, 654-666.

Derakhshandeh, J., Arjomandi M., Dally B. and Cazzolato B. (2016), "Flow-induced vibration of an elastically mounted airfoil under the influence of the wake of a circular cylinder", *Exp. Therm. Fluid Sci.*, **74**, 58-72.

Derakhshandeh, J., Arjomandi, M., Cazzolato, B. and Dally, B. (2015), "Harnessing hydro-kinetic energy from wake-induced vibration using virtual mass spring damper system", *Oean Eng.*, **108**, 115-128.

Durao, D., Heitor, M. and Pereira, J. (1988), "Measurements of turbulent and periodic flows around a square cross-section cylinder", *Exp. Fluids*, **6**(5), 298-304.

Grass, A., Raven, P., Stuart, R. and Bray, J. (1984), "The influence of boundary layer velocity gradients and bed proximity on vortex shedding from free spanning pipelines", *J. Energ, Resour, Technol.*, **106**(1), 70-78.

Hourigan, K., Thompson, M. and Tan, B. (2001), "Self-sustained oscillations in flows around long blunt plates", *J. Fluid. Struct.*, **15**(3-4), 387-398.

Lee, B.E. (1975), "The effect of turbulence on the surface pressure field of a square prism", *J. Fluid Mech.*, **69**, 263-282.

Lei, C., Cheng, L. and Kavanagh, K. (1999), "Re-examination of the effect of a plane boundary on force and vortex shedding of a circular cylinder", *J. Wind Eng. Ind. Aerod.*, **80**(3), 263-286.

Mahir, N. (2009), "Three-dimensional flow around a square cylinder near a wall", *Ocean Eng.*, **36**(5), 357-367.

Martinuzzi, R., Bailey, S. and Kopp, G. (2003), "Influence of wall proximity on vortex shedding from a square cylinder", *Exp. Fluids*, **34**(5), 585-596.

Mills, R., Sheridan, J. and Hourigan, K. (2002), "Response of base suction and vortex shedding from rectangular prisms to transverse forcing", *J. Fluid. Mech.*, **461**, 25.

Mills, R., Sheridan, J. and Hourigan, K. (2003), "Particle image velocimetry and visualization of natural and forced flow around rectangular cylinders", *J. Fluid Mech.*, **478**, 299.

Nakamura, Y., Ohya, Y. and Tsuruta, H. (1991), "Experiments on vortex shedding from flat plates with square leading and trailing edges", *J. Fluid Mech.*, **222**, 437-447.

Norberg, C. (2001), "Flow around a circular cylinder: aspects of fluctuating lift", *J. Fluid. Struct.*, **15**(3-4), 459-469.

Norberg, C. (2003), "Fluctuating lift on a circular cylinder: review and new measurements", *J. Fluid. Struct.*, **17**(1), 57-96.

Ozono, S., Ohya, Y., Nakamura, Y. and Nakayama, R. (1992), "Stepwise increase in the Strouhal number for flows around flat plates", *Int. J. Numer. Meth. Fl.*, **15**(9), 1025-1036.

Parkinson, G. (1989), "Phenomena and modelling of flow-induced vibrations of bluff bodies", *Prog. Aerosp. Sci.*, **26**(2), 169-224.

Price, S., Sumner D., Smith J., Leong K. and Paidoussis, M. (2002), "Flow visualization around a circular cylinder near to a plane wall", *J. Fluid. Struct.*, **16**(2), 175-191.

Sarkar, S. and Sarkar, S. (2010), "Vortex dynamics of a cylinder wake in proximity to a wall", *J. Fluid. Struct.*, **26**(1), 19-40.

Sohankar, A., and Etminan, A. (2009), "Forced-convection heat transfer from tandem square cylinders in cross flow at low Reynolds numbers", *Int. J. Numer. Meth. Fl.*, **60**, 733-751.

Sohankar, A., Norberg, C. and Davidson, L. (1999), "Numerical simulation of flow past a square cylinder", *Proceedings of the FEDSM99-7172—3rd ASME/JSME Joint Fluids Engineering Conference.*

Tan, B., Thompson, M. and Hourigan, K. (2003), "Sources of acoustic resonance generated by flow around a long rectangular plate in a duct", *J. Fluid. Struct.*, **18**(6), 729-740.

Taniguchi, S. and Miyakoshi, K. (1990), "Fluctuating fluid forces acting on a circular cylinder and interference with a plane wall", *Exp. Fluids*, **9**(4), 197-204.

Wang, X., Hao, Z. and Tan, S. (2013), "Vortex-induced vibrations of a neutrally buoyant circular cylinder near a plane wall", *J. Fluid. Struct.*, **39**, 188-204.

West, G.S. and Apelt, C.J. (1982), "The effect of tunnel blockage and aspect ratio on mean flow past a circular cylinder with Reynolds Number between 104 to 105", *J. Fluid Mech.*, **14**, 361-377.

Williamson, C. and Govardhan, R. (2004), "Vortex-induced vibrations", *Annu. Rev. Fluid Mech,*, **36**, 413-455.

Wu, K. (1999), "An experimental investigation of the flow around a two-dimensional cylinder in the proximity of a solid wall: effect of the gap size", MESc thesis, Faculty of Engineering Science, The University of Western Ontario, London, Canada.

Zdravkovich, M. (1997), "Flow around circular cylinders; vol. I

fundamentals", *J. Fluid Mech*., **350**(1), 377-378.

Zheng, Q., and Alam, M.M., (2017), "Intrinsic features of flow past three square prisms in side-by-side arrangement", *J. Fluid Mech*., **826**, 996-1033.